Nonlinear Mechanisms of Filamentation in Broad-Area Semiconductor Lasers

John R. Marciante and Govind P. Agrawal, *Fellow, IEEE*

Abstract— **There are three nonlinear mechanisms that can lead to filamentation in broad-area semiconductor lasers: gain-saturation-induced changes in the refractive index through the linewidth-enhancement factor, self-focusing due to heat-induced index changes, and self-defocusing through intensity-dependent index changes in the cladding layer. We present a theoretical model to analyze these mechanisms and their relative roles in destabilizing the laser output. We find that there exists a critical value for the linewidth-enhancement factor below which broad-area lasers are stable for wide stripe widths (as wide as 250 μm) and high pumping levels (as high as 20 times threshold). We also find that broad-area lasers are less susceptible to filamentation through self-defocusing and show how an intensity-dependent index in the cladding layer may be used to suppress filamentation caused by the linewidth-enhancement factor.**

I. Introduction

LATERAL instabilities have caused difficulties in the scaling of the output of semiconductor lasers to high powers. For broad-area gain regions, the light has no lateral confinement, so any increase in the local refractive index can lead to self-focusing, which breaks up the lateral mode profile into multiple filaments through a phenomenon known as beam filamentation. This phenomenon has been known for more than twenty-five years and was the main reason for the development of narrow-stripe semiconductor lasers in which the lateral mode is confined to the stripe center through gain- or index-guiding. The filamentation issue has resurfaced again in the context of MOPA (master oscillator/power amplifier) devices in which the output of a narrow-stripe, index-guided, master oscillator is amplified into a tapered-stripe power amplifier [1], [2]. Recent studies have discussed the growth and formation of filamentation in broad-area semiconductor laser amplifiers [3]–[6].

In this paper, we focus on broad-area lasers, and concentrate on three different nonlinear mechanisms. The first mechanism is the carrier-induced index change, which can occur when the local gain becomes saturated (i.e., spatial hole burning). The second is the thermally induced, intensity-dependent refractive index, which causes positive changes in the refractive index at local "hot spots" in the lasing field. The third mechanism is the self-defocusing type of nonlinearity of the cladding layers that should be included since a large part of the lateral mode resides inside the transparent cladding layers [7]. We numerically explore the limits that these nonlinearities impose on the stable output of broad-area lasers. Our numerical model is quite general as it considers the simultaneous propagation of both forward and backward waves and includes lateral variations of both the optical field and the carrier density.

This paper is organized as follows. In Section II, we present our theoretical model and introduce the nonlinear coupled differential equations that are solved numerically. Section III focuses on the first mechanism of filamentation related to the coupling of the laser field and the carrier density through the linewidth-enhancement factor. Section IV considers both self-focusing and self-defocusing nonlinearities through the intensity-dependent refractive index. Section V is devoted to the discussion and conclusion of our main results.

II. Theoretical Model

Fig. 1 shows schematically the geometry and the notation used for modeling a semiconductor laser of length L and stripe width w. The reflectivities of the laser facets located at $z = 0$ and $z = L$ are R_0 and R_L, respectively. The laser is pumped at a constant current and is assumed to be operating continuously (cw operation) in a single longitudinal mode at frequency ω. Since we are looking to solve for the lateral distribution (along the x axis) of the intracavity field, we decompose the electric field in terms of counterpropagating waves as

$$\vec{E}(\vec{r},t) = \frac{1}{2}\hat{x}\phi(y)[E_f(x,z)\exp(ikz) + E_b(x,z)\exp(-ikz)]\exp(-i\omega t) + \text{c.c.}, \tag{1}$$

where E_f and E_b represent the forward and backward traveling waves of frequency ω, respectively, $\hat{x}$ is the polarization unit vector, $k = n_{\text{eff}}k_0$ is the mode propagation constant, n_{eff} is the effective index of refraction, and $k_0 = \omega/c$ is the free-space propagation constant. Since the active layer is planar, the x and z dependence of the transverse field distribution $\phi(y)$ can be neglected. The laser field in the cavity must satisfy the wave equation

$$\nabla^2\vec{E}(\vec{r},t) - \frac{\varepsilon(\vec{r})}{c^2}\frac{\partial^2\vec{E}}{\partial t^2} = 0, \tag{2}$$

where $\varepsilon(\vec{r})$ is the complex dielectric constant whose y dependence is responsible for waveguiding in the transverse direction.

Substituting (1) into (2), making the paraxial approximation, and using the fact that $\phi(y)$ satisfies a Helmholtz equation [8],

Manuscript received July 17, 1995; revised December 1, 1995.

J. R. Marciante is with the Institute of Optics, University of Rochester, Rochester, NY 14627 USA and the Semiconductor Laser Branch, USAF Phillips Laboratory, Kirtland AFB NM 87117-5776 USA.

G. P. Agrawal is with the Institute of Optics, University of Rochester, Rochester, NY 14627 USA.

Publisher Item Identifier S 0018-9197(96)02565-1.

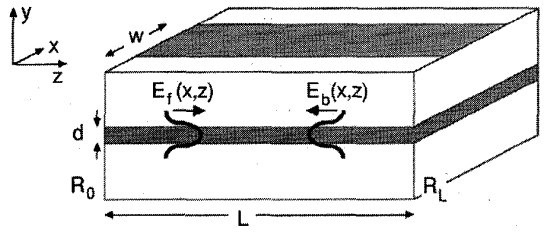

Fig. 1. Schematic illustration of the broad-area laser and the geometry used for modeling. The output facet is located at $z = L$.

the counterpropagating waves are found to satisfy a set of two coupled equations given by

$$\frac{\partial E_f}{\partial z} = \frac{i}{2k}\frac{\partial^2 E_f}{\partial x^2} + \left[\frac{1}{2}\Gamma(1 - i\alpha)g(N) - \frac{\alpha_{\text{int}}}{2} + in_2 k_0\left(|E_f|^2 + 2|E_b|^2\right)\right]E_f, \quad (3a)$$

$$-\frac{\partial E_b}{\partial z} = \frac{i}{2k}\frac{\partial^2 E_b}{\partial x^2} + \left[\frac{1}{2}\Gamma(1 - i\alpha)g(N) - \frac{\alpha_{\text{int}}}{2} + in_2 k_0\left(|E_b|^2 + 2|E_f|^2\right)\right]E_b, \quad (3b)$$

where Γ is the transverse confinement factor, α is the linewidth-enhancement factor, α_{int} is internal loss, n^2 is the Kerr coefficient [9], and $g(N)$ is the local carrier-dependent gain assumed to be $g(N) = a(N - N_0)$. Here, a is the gain cross-section, and N_0 is the transparency value for the carrier density ($g = 0$ at $N = N_0$). Equation (3) not only accounts for coupling between counterpropagating waves but also includes diffraction, carrier-induced index variations, free-carrier absorption, material gain, and self-focusing ($n_2 > 0$) or self-defocusing ($n_2 < 0$) through a Kerr-type nonlinearity. We refrain from calling α the anti-guiding parameter since it guides the light when the local carrier density drops below the average carrier density.

The carrier density distribution can be accounted for by solving the diffusion equation [10]

$$D\nabla^2 N(\vec{r}) = -\frac{J(\vec{r})}{qd} + \frac{N(\vec{r})}{\tau_{\text{nr}}} + BN^2(\vec{r}) + \frac{g(N)}{\hbar\omega}|\vec{E}(\vec{r},t)|^2, \quad (4)$$

where D is the diffusion constant, $J(\vec{r})$ is the injected current density, q is the magnitude of the electron charge, d is the active-layer thickness, τ_{nr} is the nonradiative lifetime, and B is the spontaneous-emission coefficient. The first term accounts for carrier injection, while the second and third terms account for the nonradiative and spontaneous recombinations, respectively. The last term is due to stimulated recombination and accounts for gain saturation.

By using (1) and making several simplifying assumptions, we can rewrite (4) in the form

$$D\frac{\partial^2 N(x,z)}{\partial x^2} = -\frac{J(x,z)}{qd} + \frac{N(x,z)}{\tau_{\text{nr}}} + BN^2(x,z) + \frac{\Gamma g(N)}{\hbar\omega}\left(|E_f|^2 + |E_b|^2\right). \quad (5)$$

Three assumptions were made in obtaining (5). The first is that the carrier density is uniform over the active-layer thickness since the active layer is very thin compared to the diffusion length ($\sim$3 μm). This allows the y dependence of the current and carrier densities to be neglected. The confinement factor Γ in (5) results from averaging along the y direction and takes into account the mode spreading outside the active layer. The second assumption is that longitudinal spatial hole burning is washed out by diffusion since the diffusion length is large compared to the lasing wavelength. This allows the rapidly-varying interference term to be dropped from the stimulated recombination term in (4). The third assumption is that axial variations of N occur over length scales much longer than the diffusion length so that the second derivative in the z direction can be neglected.

We solve (3) and (5) iteratively using a split-step Fourier (or beam propagation) method [10]–[12] iteratively, using the boundary conditions $E_f(x,0) = \sqrt{R_0}E_b(x,0)$ and $E_b(x,L) = \sqrt{R_L}E_f(x,L)$ to relate the forward and backward propagating beams at the facets. Here, R_0 and R_L represent the facet power reflectivities at $x = 0$ and $x = L$, respectively. The iteration procedure is initiated by using a rectangular lateral profile at $z = 0$. The carrier density is calculated laterally for each step in the propagation using a tridiagonal matrix method. Our convergence criteria rest on comparing the changes in the output power and the lateral mode width on successive round trips. Depending on the laser parameters, the iteration procedure either converges (typically within 30–40 round trips) or fails to converge even after hundreds of round trips. The lateral mode is identified as unstable in the latter case. Unstable or nonconvergent lateral profiles are obtained by averaging over five iterations after 100 nonconvergent round-trip iterations have been made. Since each iteration corresponds to about 6 ps (round-trip time), this window represents a $\sim$30 ps slice in time, which is resolvable on a 30 GHz detector. Thus, for our model, the unstable profiles are representative of a snapshot at some time after the relaxation oscillation transients have died out. The parameter values used for numerical simulations are displayed in Table I. These values are appropriate for an AlGaAs semiconductor laser operating near 820 nm. The qualitative trends of the results obtained here are, however, applicable to any semiconductor laser, including quantum-well devices.

For numerical purposes, it is useful to show results as a function of J/J_{th}, where J is constant over the stripe width w and zero outside the stripe, and J_{th} is the threshold current density. Since the field is negligible below threshold, the last term in (5) can be neglected. However, J_{th} depends on the stripe width w because of carrier diffusion. For simplicity, we solve for the threshold current density from (5) by neglecting carrier diffusion. The result is $J_{\text{th}} = (qdN_{\text{th}}/\tau_{\text{nr}})\,[1 + B\tau_{\text{nr}}N_{\text{th}}]$, where $N_{\text{th}} = N_0 + (\alpha_{\text{mir}} + \alpha_{\text{int}})/(a\Gamma)$ with $\alpha_{\text{mir}} = -\ln(R_0R_L)/L$ can be obtained by equating the gain and losses of the system [8]. This simple model of threshold does not apply for narrow stripes ($\lesssim$10 μm) that can yield device thresholds higher than the calculated value (because of carrier diffusion), but it allows us to define a pump parameter $r = J/J_{\text{th}}$ that is constant with respect to the stripe width.

TABLE I
PARAMETERS VALUES USED IN NUMERICAL SIMULATIONS

Physical quantity	Symbol	Value
Cavity length	L	250 μm
Contact stripe width	w	variable
Active-layer thickness	d	200 nm
Transverse confinement factor	Γ	0.2
Facet power reflectivities	R_0, R_L	0.35
Laser wavelength	λ	820 nm
Effective index	n_{eff}	3.5
Kerr coefficient	n_2	variable
Linewidth-enhancement factor	α	variable
Internal loss	α_{int}	10 cm^{-1}
Gain cross-section	a	1.5 x 10^{-16} cm^2
Diffusion constant	D	33 cm^2/s
Transparency carrier density	N_0	1.0 x 10^{18} cm^{-3}
Non-radiative lifetime	τ_{nr}	5 ns
Spontaneous-emission coefficient	B	1.4 x 10^{-10} cm^3/s

This is equivalent to scaling the total injected current directly with the stripe width. In Sections III and IV, the numerical results are presented by varying $r = J/J_{\rm th}$ in the range 1–20.

III. INSTABILITY DUE TO CARRIER-INDUCED INDEX CHANGES

For gain-guided lasers, there is no critical stripe width that selects only one lateral mode [8]. However, for narrow enough stripe widths, there can be stable operation, even in the presence of spatial hole burning. As a representative example of stable operation, Fig. 2(a) shows the lateral intensity (solid curve) and carrier density (dashed curve) profiles at the output facet for an 8-μm width stripe when the laser is operating at three times above threshold ($r = 3$), while Fig. 2(b) shows the corresponding far-field distribution. Spatial hole burning is clearly seen in Fig. 2(a). Also seen in Fig. 2(b) is the evidence of "rabbit ears" in the far field, a well-known feature of narrow-stripe semiconductor lasers that is attributed to astigmatism induced by the linewidth-enhancement factor [13]. As the stripe width increases for a constant current density, the "rabbit ears" in the far field become less pronounced, but both the near and far fields remain symmetric. Beyond a critical value of the stripe width, a phase-transition-like behavior is observed in the sense that both near and far fields become asymmetric and, at the same time, the lateral profile becomes unstable. Fig. 3(a) shows a snapshot of the lateral profile in the unstable region for $w = 14$ μm. The lack of symmetry is clearly evident in the near field. This asymmetry is also present in the phase profile, which produces an asymmetric far-field distribution, shown in Fig. 3(b). Since a steady state is not reached for $w = 14$ μm, both near- and far-field profiles change on successive round trips, but they remain asymmetric. Note that the minima in the carrier density profile (dashed curve) in Fig. 3(a) does not always correspond with the maxima in the intensity profile. The reason for this behavior rests on the stripe-edge effects; for narrow stripes, the carrier density decreases monotonically past the stripe edge due to diffusion and lack of pumping.

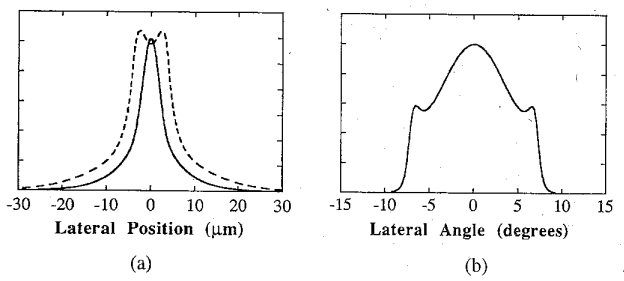

Fig. 2. Lateral profiles for an 8-μm stripe-width laser operating at three times above threshold with $\alpha = 3$. (a) Profiles at the output facet for near field intensity (solid curve) and carrier density (dashed curve). (b) Far-field intensity distribution. A normalized vertical scale is used in each case.

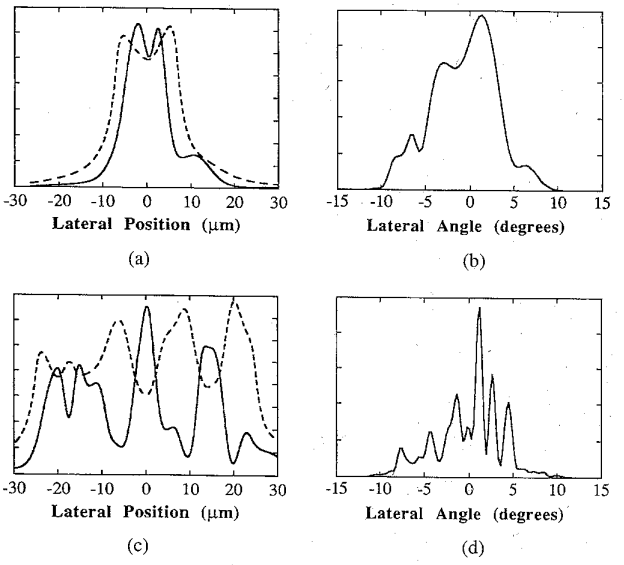

Fig. 3. Same as in Fig. 2 except the stripe width has been changed to 14 μm (upper row) and 50 μm (lower row).

Fig. 3(c) and (d) shows the near and far fields for a stripe width of 50 μm. For such a wide stripe, the filaments are fully developed. The major filament structures are spaced by about 15 μm, in agreement with the experimental observations found in the literature [14]–[16]. The carrier density (dashed curve) in Fig. 3(c) shows an anticorrelation of peaks with those of the near-field distribution, as expected from spatial hole burning. The amplitude-phase coupling, via the linewidth-enhancement factor, produces a multi-lobed far-field pattern shown in Fig. 3(d).

The near and far fields shown in Fig. 3 correspond to the laser output from the facet at $z = L$. We expect the intracavity lateral mode and carrier density profiles to change along the cavity length. Fig. 4 shows the intracavity intensity as a "grayscale" plot for the case of the 50-μm-wide stripe. The three major filaments (seen at the output in Fig. 3(c)) exist throughout the cavity. Although beam steering is evident, the light diverges only at small angles, so our assumption of paraxial propagation for the fields in (1) remains valid. This figure also shows that the mean-field approximation that is often used in broad-area laser calculations [17], [18] may be questionable.

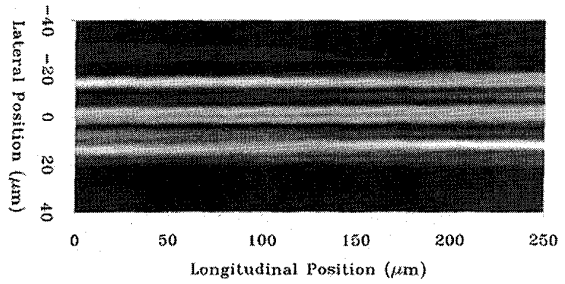

Fig. 4. Intracavity axial variation of the lateral intensity distribution for the 50-μm stripe. In the grayscale plot, light regions represent high intensities while dark regions represent low intensities.

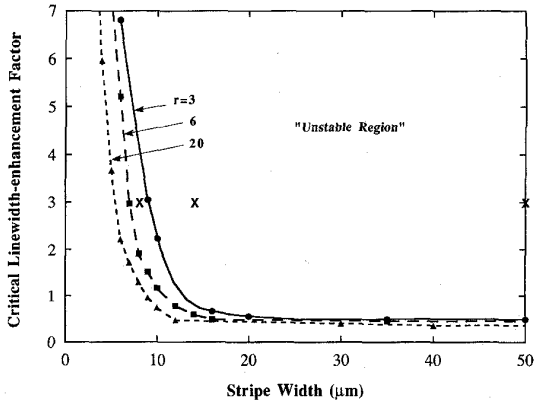

Fig. 5. Stable operation boundaries in the w-α plane. The curves are critical values of α for which the lateral mode becomes unstable at a given stripe width w for $r = 3$ (solid curve), $r = 6$ (dashed curve), and $r = 20$ (dotted curve). The crosses correspond to the operating parameters used in Figs. 2 and 3 with $r = 3$.

The results shown in Figs. 2–4 are obtained for a fixed value of $\alpha = 3$. It is well known that the linewidth-enhancement factor α plays an important role in destabilizing the lateral mode and producing filamentation [5], [17]. We have seen that for a given value of α, there is some width at which the lateral profile becomes unstable. Conversely, for a given stripe width w, we can find a critical value of the linewidth-enhancement factor that will destablilize the laser. Fig. 5 shows the regions of stable and unstable operations in the w-α plane for three different applied current densities. Several conclusions can be drawn from Fig. 5. First, semiconductor lasers with any value of α are stable for narrow stripes ($\lesssim$6 μm). Second, the critical width at which the device will operate stably depends on the level of pumping; increased levels of pumping reduce the critical width at which a laser can operate stably. Third, for a given pump level, variations in α around typical device values ($\alpha \sim$ 2–5) do not change this critical stripe width much, and this feature has been noted in practice for device fabrication. Fourth, for wide stripes, the critical linewidth-enhancement factor below which the laser operates stably remains fairly constant and is not affected much by different injected current densities. We have verified numerically that this behavior persists for stripes as wide as 250 μm. A key feature of Fig. 5 is that for values of the linewidth-enhancement factor below 0.4, the laser will remain stable for very wide stripe widths at a pumping level as high as 20 times threshold.

The points displayed by crosses in Fig. 5 correspond to the values of α and w used to calculate the lateral profiles shown in Figs. 2 and 3. For the parameter values given in Table I, the current densities of 11.9 kA/cm^2, 23.7 kA/cm^2, and 79.1 kA/cm^2 correspond to operating at three times, six times, and twenty times above threshold, respectively.

IV. Instability Due to Self-Focusing and Self-Defocusing

As mentioned earlier, both self-focusing and self-defocusing, governed by the parameter n_2 in (3), can also destabilize the lateral laser mode. Although, in practice, both α and n_2 are nonzero for semiconductor lasers, we first set the linewidth-enhancement factor to zero to isolate the role of n_2 in the destabilization of the laser.

We examine the regions of instability as we did for the linewidth-enhancement factor, calculating the critical value of n_2 which will destabilize the laser of a certain stripe width w. However, the Kerr coefficient n_2 can be positive or negative, causing self-focusing or self-defocusing, respectively (see (3)). Fig. 6 shows the regions of stable and unstable operation by plotting the value of n_2 for which the lateral mode becomes unstable for a given stripe width for the same three different current densities used in Fig. 5. Consider first the self-focusing case of $n_2 > 0$. The critical n_2 curves display a qualitatively similar behavior as the critical α curves in Fig. 5. For narrow stripes, there is stable operation, and for wide stripes, there is also stability if n_2 is below some constant critical value. However, unlike the critical α curves, variations in n_2 do change considerably the critical stripe width for stable operation; the phase-transition region has a less steep slope than the corresponding region in the critical α curves. Also, the pumping level strongly affects the stability of the device. Higher pumping levels drastically reduce the slope of the phase-transistion region. And even though the critical n_2 remains constant at wide stripe widths, it decreases as the applied current density is increased. This can be understood by noting that the nonlinear index shift is given by $n_2 I$, where I is the local intensity of the lasing field. The effect here is not as large in Fig. 5 since the linewidth-enhancement factor causes a nonlinear index shift proportional to $\alpha \Delta N$, and the depth of modulation of the carrier density due to spatial hole burning is not as large as the depth of modulation in the lasing field, as displayed in Fig. 3(c). This phenomenon arises from the interplay between the carrier density and the lasing field; a small variation in N around N_{th} will cause the field intensity to be modulated by 100% as the gain is switched on and off.

Next, we turn our attention to the self-defocusing case of $n_2 < 0$. Intuitively, one might expect that self-defocusing should not lead to filamentation. However, Fig. 6 clearly shows that sufficient self-defocusing can lead to lateral instability. The self-defocusing curves are quite similar in behavior to those of the self-focusing case, with variations in the pumping level having the same effects. Fig. 6 shows that the devices are much more stable with respect to self-defocusing than to self-focusing. For similar magnitudes of n_2, the critical

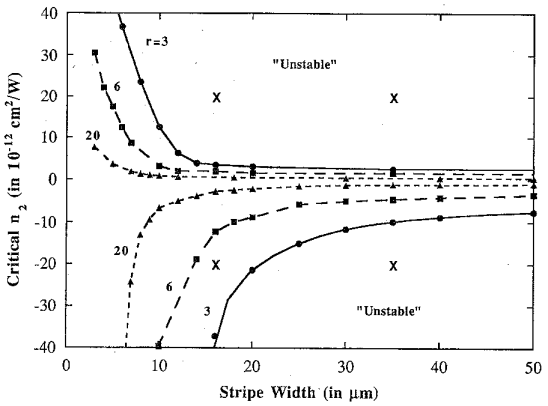

Fig. 6. Stable operation boundaries in the w-n_2 plane. The curves are critical values of n_2 for which the lateral mode becomes unstable at a given stripe width w for $r = 3$ (solid curve), $r = 6$ (dashed curve), and $r = 20$ (dotted curve). The crosses correspond to the operating parameters used in Fig. 7 with $r = 3$.

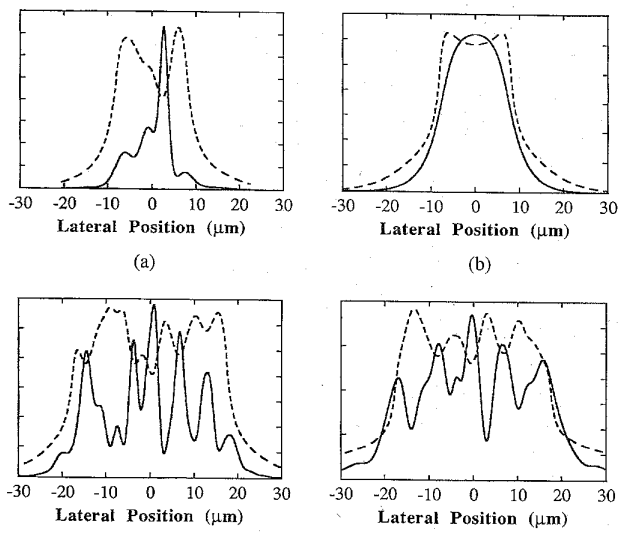

Fig. 7. Near field (solid curves) and carrier density (dashed curves) distributions for 16 μm (upper row) and 35 μm (lower row) stripe widths for $n_2 = 20 \times 10^{-12}$ cm^2/W (left column) and $n_2 = -20 \times 10^{-12}$ cm^2/W (right column). In each case, $\alpha = 0$ and $r = 3$.

stripe width at which the laser become unstable is much wider for the self-defocusing case than the self-focusing case. Also, the constant critical value of n_2 at wide stripe widths is considerably larger for the self-defocusing case. Most notable here is that there seems to be an absolute stability region for stripe widths $\lesssim 5$ μm. All of these indicators lead us to conclude that self-defocusing is much less effective than self-focusing in destabilizing the lateral mode.

An interesting point is that for identical devices, the sign of n_2 can determine whether or not the device will operate stably. Consider a stripe width of 16 μm and $r = 3$ (solid curve) in Fig. 6. For the self-focusing nonlinearity, the snapshot of the laser output in Fig. 7(a) shows the breakdown of the lateral profile at $w = 16$ μm, similar to the behavior displayed in Fig. 3(a). By contrast, the self-defocusing nonlinearity produces a stable, clean, near-field profile, displayed in Fig. 7(b). Now consider a stripe width for which either sign will produce unstable operation. At a stripe width of 35 μm, filamentation is present for both self-focusing and self-defocusing. The snapshot in Fig. 7(c) shows deep filamentation and spatial hole burning for $n_2 > 0$. For the self-defocusing case, as displayed in the Fig. 7(d) snapshot, the filamentation is not as deep. Again, this speaks for the relative stability of this device against the self-defocusing nonlinearity. An interesting point is that these cases produce filaments spaced by about 8 μm, where the filaments displayed in Fig. 3(c) are spaced by 15 μm. However, it must be noted that the filament spacing may change as the Kerr coefficient is varied.

V. Discussion and Conclusion

In this paper, we have discussed three distinct nonlinear mechanisms responsible for filamentation in broad-area semiconductor lasers. The carrier-induced index change, resulting from spatial hole burning and governed by the linewidth-enhancement factor α, is the most dominant mechanism, having an effective value for $n_2 \sim 10^{-10}$ cm^2/W (see the Appendix). Since self-defocusing introduces a negative intensity-dependent refractive index while the α-induced index change is positive, it may be possible to reduce or eliminate these lateral instabilities with the cladding-layer nonlinearity. Displayed in Fig. 8 are near-field profiles for a 50-μm wide stripe lasers operating three times above threshold with $\alpha = 3$, a typical value for the linewidth-enhancement factor. Fig. 8(b) corresponds to the case where Kerr coefficient n_2 is zero and is identical to the near field shown in Fig. 3(c), whereas $n_2 = 20 \times 10^{-12}$ cm^2/W and -20×10^{-12} cm^2/W for the near fields shown in Figs. 8(a) and (c), respectively. In the case of self-focusing (Fig. 8(a)), instability is enhanced as evidenced by the increase of filaments and subfilamentary structures. By contrast, the self-defocusing nonlinearity of the same magnitude (Fig. 8(c)) shows some stabilization compared to the $n_2 = 0$ case in Fig. (8(b)), noted by the decrease in the depth of modulation of the filaments. A case was not found to eliminate the filamentation for $\alpha = 3$, but for $\alpha = 2$, the instability was removed with a value of $n_2 \approx -5 \times 10^{-12}$ cm^2/W at a stripe width of 50 μm when the laser was operating five times above threshold ($r = 5$). A more detailed study [7] revealed that this cladding-layer nonlinearity cannot help if the linewidth-enhancement factor is much greater than two. However, for smaller values of the linewidth-enhancement factor and a limited range of operating intensity, it was possible to eliminate filamentation and stabilize the lateral mode profile.

We have shown examples of filamentation due to the linewidth-enhancement factor and regions of stability for various stripe widths and operating levels. The onset of filamentation occurs for wide stripe widths ($\gtrsim 12$ μm) and is enhanced by higher pumping levels. It was also shown that there is a value for the linewidth-enhancement factor below which the devices are stable for wide stripe widths (up to 250 μm) and high pumping levels. Unfortunately, the required value of $\alpha < 0.4$ is too low to be realistic for most semiconductor lasers. However, we should note that the effective value of

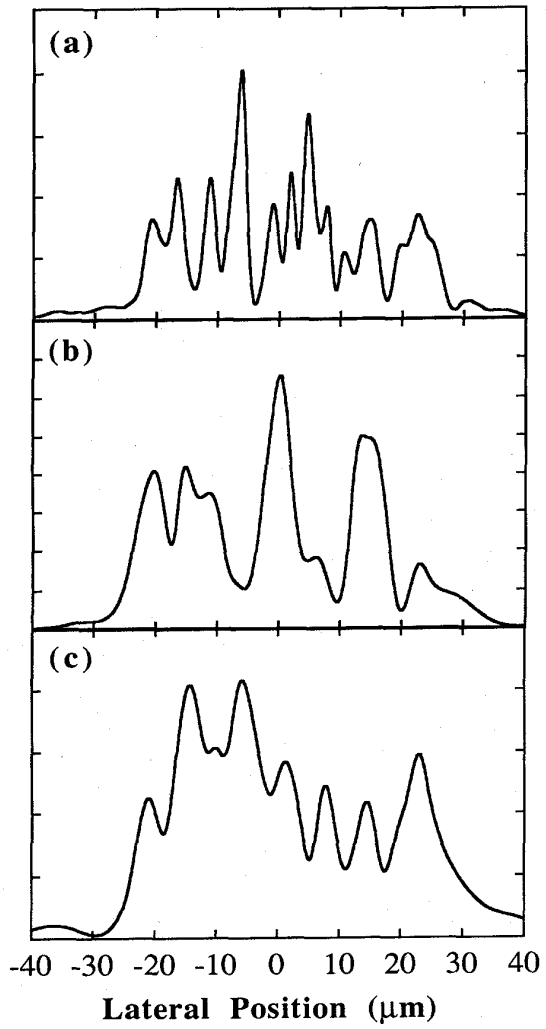

Fig. 8. Comparison of near-field intensity profiles for a 50 μm stripe width laser for (a) $n_2 = 20 \times 10^{-12}$ cm^2/W. (b) $n_2 = 0$. (c) $n_2 = -20 \times 10^{-12}$ cm^2/W. In each case, $\alpha = 3$ and $r = 3$.

α is generally different than the material value of α [19], and it may be possible to design a broad area laser such that the effective α is below the critical value. Such devices will be stable without filamentation, regardless of stripe width or injection current.

We have shown that lateral instabilities are also effected by the Kerr-type nonlinearity, governed by the intensity-dependent index of refraction. Within the active region, an important source for the positive intensity-dependent refractive index ($n_2 > 0$) has its origin in optically-induced heating [1], [5], [15]. Although there are several sources of heating within the semiconductor, such as resistive heating, most of these effects do not contain a strong lateral variation and thus will not significantly affect the lateral profile. It is difficult to estimate the effective value of n_2 for optically-induced heating because of the uncertainty in several device parameters such as the thermal resistivity. However, our rough estimate indicates that n_2 values are significantly smaller than the effective n_2 value resulting from the carrier-induced index change (see Appendix). Thermal nonlinearities may be avoided altogether by using pulses that are shorter than the thermal response time (~ms) but still longer than the carrier lifetime (~ns) so that our cw analysis presented here remains valid.

A source for the negative intensity-dependent refractive index ($n_2 < 0$) could come from the cladding layers. Since the photon energy in the cladding layers is below the bandgap, it experiences little loss. However, the third-order susceptibility still leads to an index change given as $\Delta n = (1 - \Gamma)n_2 I$, which may be nonnegligible since most of the light is in the cladding layers. Experimentally measured values of n_2 for AlGaAs near the 0.8 μm wavelength region are in the range $n_2 = -4$–8×10^{-12} cm^2/W depending on the Al content [20], [21], with similar values reported for InGaAsP near 1.5 μm [22], [23]. As seen from Fig. 6, such values are large enough to affect the lateral stability for stripe widths $\gtrsim$15 μm when the laser operates 4–6 times above threshold. By a proper design of the cladding layers, the self-defocusing nonlinearity may help to offset or even cancel the filamentary self-focusing effects caused by the linewidth-enhancement factor [7]. This same idea may also be applied to amplifier and MOPA configurations to extend the device length and thus increase the output power.

Appendix
Effective n_2 for Carrier-Induced Nonlinearity

In order to get an expression for an effective n_2 caused by the linewidth-enhancement factor, we first need to eliminate the carrier density from the gain in (3). Ignoring diffusion in (5) and assuming only small deviations in the carrier density from its threshold value, we can solve for the carrier density as

$$N = N_0 + \frac{J\tau/(qd) - N_0}{1 + I/I_s}, \tag{6}$$

where I is the intensity of the lasing field, $I_s = \hbar\omega/(a\Gamma\tau)$ is the saturation intensity, and τ is the carrier lifetime that includes nonradiative and spontaneous recombination through $1/\tau = 1/\tau_{\rm nr} + BN_{\rm th}$. Equation (6) yields a saturable form for the gain $g(N) = a(N - N_0) = g_0/(1 + I/I_s)$, where the small signal gain is given by $g_0 = a[J\tau/(qd) - N_0]$. From (3), this saturable gain yields a carrier-induced index change

$$\Delta n = -\frac{\alpha\Gamma g_0}{2k_0(1 + I/I_s)}, \tag{7}$$

where α is the linewidth-enhancement factor. Although in general, I can become comparable to the saturation intensity close to laser threshold, we can expand Δn in a Taylor series and write Δn as $\Delta n_0 + n_2 I$. The effective value of n_2 is found to be given by

$$n_2 = \frac{\alpha\Gamma g_0}{2k_0 I_s}. \tag{8}$$

Using the parameter values from Table I, we obtain $\tau = 1.9$ ns, and $I_s = 4.25$ MW/cm^2. Assuming near threshold operation and using $g_0 = 210$ cm^{-1}, the effective α-induced Kerr

coefficient is $n_2 = 1.9 \times 10^{-10}$ cm^2/W. At higher pumping levels, strictly speaking, the definition of n_2 does not remain valid. Qualitatively speaking, the effective values of n_2 should be $\sim 10^{-10}$ cm^2/W because of gain saturation.

REFERENCES

[1] L. Goldberg, M. R. Surette, and D. Mehuys, "Filament formation in tapered GaAlAs optical amplifier," *Appl. Phys. Lett.*, vol. 62, pp. 2304–2306, 1993.

[2] D. J. Bossert, J. R. Marciante, and M. W. Wright, "Feedback effects in tapered broad-area semiconductor lasers and amplifiers," *IEEE Photon. Technol. Lett.*, vol. 7, pp. 470–472, 1995.

[3] A. H. Paxton and G. C. Dente, "Filament formation in semiconductor laser gain regions," *J. Appl. Phys.*, vol. 70, pp. 1–6, 1991.

[4] M. Tamburrini, L. Goldberg, and D. Mehuys, "Periodic filaments in reflective broad area semiconductor optical amplifiers," *Appl. Phys. Lett.*, vol. 60, pp. 1292–1294, 1992.

[5] R. J. Lang, D. Mehuys, A. Hardy, K. M. Dzurko, and D. F. Welch, "Spatial evolution of filaments in broad area diode laser amplifiers," *Appl. Phys. Lett.*, vol. 62, pp. 1209–1211, 1993.

[6] R. J. Lang, D. Mehuys, D. F. Welch, and L. Goldberg, "Spontaneous filamentation in broad-area diode laser amplifiers," *IEEE J. Quantum Electron.*, vol. 30, pp. 685–693, 1994.

[7] J. R. Marciante and G. P. Agrawal, "Controlling filamentation in broad-area semiconductor lasers and amplifiers," *Appl. Phys. Lett.*, to be published.

[8] G. P. Agrawal and N. K. Dutta, *Semiconductor Lasers*, 2nd ed. New York: Van Nostrand Reinhold, 1993.

[9] N. Peyghambarian, S. W. Koch, and A. Mysyrowicz, *Introduction to Semiconductor Optics*. Englewood Cliffs, NJ: Prentice-Hall, pp. 340–342, 1993.

[10] G. P. Agrawal, "Fast-Fourier-transform based beam-propagation model for stripe-geometry semiconductor lasers: Inclusion of axial effects," *J. Appl. Phys.*, vol. 56, pp. 3100–3109, 1984.

[11] M. Lax, J. H. Batteh, and G. P. Agrawal, "Channeling of intense electromagnetic beams," *J. Appl. Phys.*, vol. 52, pp. 109–125, 1981.

[12] G. C. Dente and M. L. Tilton, "Modeling broad-area semiconductor optical amplifiers," *IEEE J. Quantum Electron.*, vol. 20, pp. 76–88, 1993.

[13] G. P. Agrawal, "Effect of index guiding on the far-field distribution of stripe-geometry lasers," *Opt. Commun.*, vol. 47, pp. 283–287, 1983.

[14] R. J. Lang, A. G. Larsson, and J. G. Cody, "Lateral modes of broad area semiconductor lasers: Theory and experiment," *IEEE J. Quantum Electron.*, vol. 27, pp. 312–320, 1991.

[15] J. P. Hohimer, G. R. Hadley, and A. Owyoung, "Mode control in broad-area diode lasers by thermally induced lateral index tailoring," *Appl. Phys. Lett.*, vol. 52, pp. 260–262, 1988.

[16] I. Fischer, O. Hess, and W. Elsässer, "Spatio-temporal dynamics in a broad area laser diode," *Nonlinear Dynamics in Optical Systems*, Rochester, NY, paper TD2, June 5–7, 1995.

[17] H. Adachihara, O. Hess, E. Abraham, P. Ru, and J. V. Moloney, "Spatiotemporal chaos in broad-area semiconductor lasers," *J. Opt. Soc. Am. B*, vol. 10, pp. 658–665, 1993.

[18] O. Hess, S. W. Koch, and J. V. Moloney, "Filamentation and beam propagation in broad-area semiconductor lasers," *IEEE J. Quantum Electron.*, vol. 31, pp. 35–43, 1995.

[19] S. S. Lee, L. Figueroa, and R. Ramaswamy, "Variations of linewidth enhancement factor and linewidth as a function of laser geometry in (AlGa)As Lasers," *IEEE J. Quantum Electron.*, vol. 25, pp. 862–870, 1989.

[20] M. J. LaGasse, K. K. Anderson, C. A. Wang, H. A. Haus, and J. G. Fujimoto, "Femtosecond measurements of the nonresonant nonlinear index in AlGaAs," *Appl. Phys. Lett.*, vol. 56, pp. 417–419, 1990.

[21] G. I. Stegeman, "Nonlinear guided wave optics," *Contemporary Nonlinear Optics*, G. P. Agrawal and R. W. Boyd, Eds. New York: Academic, 1992, ch. 1.

[22] K. L. Hall, A. M. Darwish, E. P. Ippen, U. Koren, and G. Raybon, "Femtosecond index nonlinearities in InGaAsP optical amplifiers," *Appl. Phys. Lett.*, vol. 62, pp. 1320–1322, 1993.

[23] A. D'Ottavi, E. Iannone, A. Mecozzi, S. Scotti, P. Spano, R. Dall'Ara, G. Guekos, and J. Eckner, "4.3 terahertz four-wave mixing spectroscopy of InGaAsP semiconductor amplifiers," *Appl. Phys. Lett.*, vol. 65, pp. 2633–2635, 1994.

John R. Marciante received the B.S. degree in engineering physics from the University of Illinois at Urbana-Champaign in 1991. Under the Palace Knight program, he joined the Phillips Laboratory, Kirtland AFB, NM, and started his graduate studies at the Institute of Optics at the University of Rochester. In 1992, he received the M.S. degree in optics and initiated work towards the Ph.D. degree.

He spent a year at the Phillips Laboratory working in the Semiconductor Laser Branch and resumed graduate work in 1994 at the Institute of Optics, where he currently is pursuing the Ph.D. degree. His research interests include high-power semiconductor and solid-state laser systems, quantum and electro-optics, and nonlinear optics. Currently, his thesis work is focused on dynamic filamentation and spatial feedback effects in semiconductor lasers, and phase conjugation in semiconductor materials for applications towards semiconductor laser arrays.

Govind P. Agrawal (M'83–SM'86–F'96) received the B.S. degree from the University of Lucknow in 1969 and the M.S. and Ph.D. degrees from the Indian Institute of Technology, New Delhi, in 1971 and 1974, respectively.

After holding positions at the Ecole Polytechnique, France, the City University of New York, and AT&T Bell Laboratories, Murray Hill, NJ, he joined in 1989 the faculty of the Institute of Optics at the University of Rochester where he is a Professor of Optics. His research interests focus on quantum electronics, nonlinear optics, and laser physics. In particular, he has contributed significantly to the fields of semiconductor lasers, nonlinear fiber optics, and optical communications. He is an author or coauthor of more than 200 research papers, several book chapters and review articles, and three books entitled *Semiconductor Lasers* (New York: Van Nostrand, 1993), *Nonlinear Fiber Optics* (New York: Academic, 1995), and *Fiber-Optic Communication Systems* (New York: Wiley, 1992). He has also edited the books, *Contemporary Nonlinear Optics* (New York: Academic, 1992) and *Semiconductor Lasers: Past, Present and Future* (AIP Press, 1995).

Dr. Agrawal is a Fellow of the Optical Society of America (OSA).